

Fully Differential Soft Gluon Evolution at the Amplitude Level

Jeffrey R. Forshaw,^a Simon Plätzer,^{b,c} and Fernando Torre González^a

^a*Department of Physics and Astronomy, University of Manchester, Manchester M13 9PL, United Kingdom*

^b*Institute of Physics, NAWI Graz, University of Graz, Universitätsplatz 5, A-8010 Graz, Austria*

^c*Particle Physics, Faculty of Physics, University of Vienna, Boltzmannngasse 5, A-1090 Wien, Austria*

E-mail: jeffrey.forshaw@manchester.ac.uk, simon.plaetzer@uni-graz.at,
fernando.torre@manchester.ac.uk

ABSTRACT: We study differential intra-jet radiation patterns in jet production at full colour. We present a systematic study of several QCD $2 \rightarrow 2$ processes and also multi-jet production from a colourless initial state. We examine how subleading colour corrections are distributed differentially in phase space and find that mere normalization effects due to subleading colour can be due to subtle cancellations across phase space. In general, we find that subleading colour does affect the shapes of distributions.

Contents

1	Introduction	1
2	Fully differential soft gluon evolution	2
3	Final state jets	4
4	Hadronic jets	7
4.1	Back-to-back jets	8
4.2	Jets with a boost	10
4.3	Jets with a recoil	14
5	Conclusions and outlook	15
A	Coulomb gluon exchange	17

1 Introduction

In a partner paper [1], we presented a systematic and comprehensive analysis of sub-leading colour corrections in perturbative QCD processes involving multiple soft gluon emissions. In that paper, we used a dedicated module of the `CVolver` code [2, 3] to study jet veto cross sections for a range of partonic scattering processes. In this work, we extend the scope of the analysis by employing `CVolver` as a partonic event generator in order to study a broader class of jet observables, enabling a comprehensive investigation of colour evolution effects across a variety of final-state configurations. Specifically, we consider observables fully differential in the kinematics of the highest energy gluon emitted outside of the primary jets. This allows us to explore how sub-leading colour effects are distributed in phase space and to perform a first investigation into what observables (other than veto cross sections) may pick up substantial corrections. This work is an important step on the way to a complete, multi-purpose event generator operating at full colour accuracy.

The remainder of this paper is structured as follows. In the next section we introduce the observables that will be the focus of the rest of the paper. For the case of the jet veto cross section, we show that the event generator mode delivers identical results to those reported in the partner paper, obtained using the dedicated mode. This constitutes a highly non-trivial check of the event generator mode. In Section 3 we consider hard scattering processes with no incoming coloured particles, such as occur in e^+e^- collisions. We consider four-parton final states, e.g. as in W^+W^- or ZZ decay, and are able to account for colour interference and reconnection effects. In Section 4 we consider a range of two-to-two hard scattering processes in a variety of kinematic configurations. Section 5 forms our conclusions.

For details of the theoretical framework underpinning this analysis we refer to the partner paper [1] and also references [3–5]. The key point to appreciate is that `CVolver` is able to resum leading soft gluon emissions to a prescribed accuracy in $1/N_c$ by evolving at the amplitude level.

2 Fully differential soft gluon evolution

We use a soft gluon evolution equation with an infrared cutoff in both energy and collinearity. Presently, we only consider observables that are completely collinear safe and inclusive in soft gluon emissions below a characteristic scale, i.e. those observables that are only sensitive to wide-angle soft gluon emissions. Observables that involve logarithmic sensitivity to the angular cutoff need to be evolved with a collinear anomalous dimension [5, 6], a study which we defer to a future publication in which also hard collinear contributions will be addressed. Observables sensitive to wide-angle soft gluon emissions include jet veto cross sections and, more generally, the triple-differential cross section:

$$\frac{d^3\sigma}{d\Omega d\rho} = \sum_n \int d\sigma_n \delta(\rho - E_i) \delta(\Omega - \Omega_i) , \quad (2.1)$$

where i labels the soft gluon with the highest energy (ρ) that is emitted in what we refer to as the veto region, i.e. outside of the regions we identify with jets. Our choice of the veto region will be process dependent but is always such that it avoids the regions collinear to the hard partons. A number of interesting observables can be derived from this differential cross section. In particular we consider:

$$\frac{d^2\Sigma(r)}{d\Omega} = \int_0^r d\rho \frac{d^3\sigma}{d\Omega d\rho} \quad (2.2)$$

$$\frac{d\Sigma(r)}{d\cos\theta} = \int_0^{2\pi} \int_0^r d\rho d\phi \frac{d^3\sigma}{d\Omega d\rho} \quad (2.3)$$

$$\frac{d\Sigma(r)}{d\phi} = \int_{-1}^1 \int_0^r d\rho d(\cos\theta) \frac{d^3\sigma}{d\Omega d\rho} . \quad (2.4)$$

We do not perform a normalization of the resulting cross section to the full colour inclusive cross section of the hard process, allowing subleading colour contributions to change the normalization as we include higher orders in $1/N_c$. Integrating Eq. (2.2) over the veto region gives the ‘gaps-between-jets’ cross section with veto energy r . One key test of the event generator mode will be to confirm that doing this integral reproduces the results in [1, 3]. Note that since we do not include hard-collinear physics the inclusion of Coulomb (Glauber) gluon exchanges will lead to super-leading logarithms regulated by the collinear cutoff. As a result, we turn off Coulomb exchanges for the present paper and will return to perform a more comprehensive study including their effects in the future. That said, in Appendix A, we do show some results for the jet veto cross section. We intend to explore the effects of Coulomb exchanges more fully in an upcoming study.

We use `CVolver` to generate events with gluon energies greater than $\mu = 0.1$ (in units of the maximum gluon energy) and with a collinear cutoff as described in [1]. The collinear

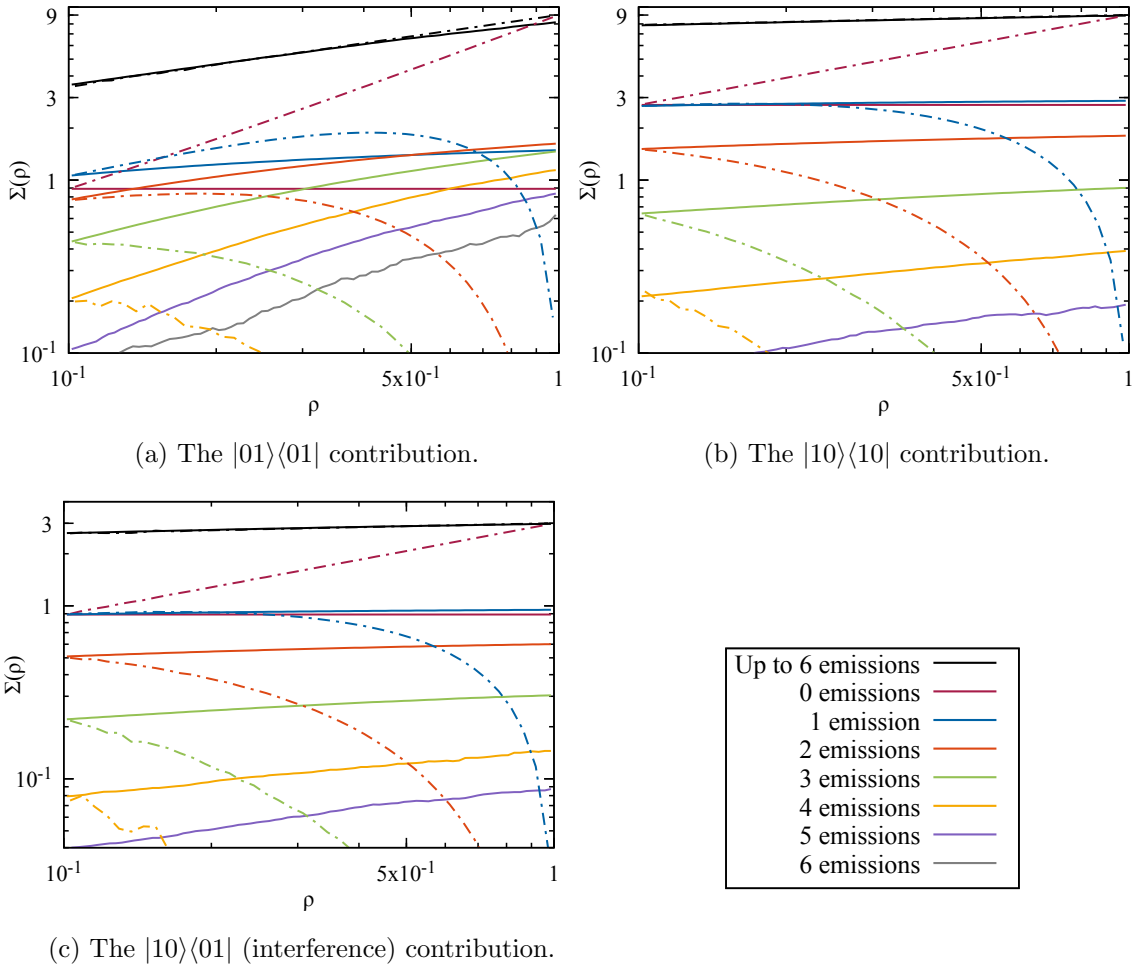


Figure 1: Comparison of the event generator and dedicated modes of `CVolver`, for the $q\bar{q} \rightarrow q\bar{q}$ process with kinematics and colour flows explained in the text. The solid curves are the full colour event generator evolution and the dash-dotted curves are the full colour dedicated mode evolution.

cutoff is always chosen to be sufficiently small as to guarantee our results are independent of it. For the hard scatter process, we consider a variety of partonic processes each with fixed kinematics. Apart from the energy and collinear cutoffs, there are no other generator-level cuts, which means we are fully differential in the final state phase space, though for this paper we will focus on the observables defined in equations (2.2)–(2.4).

An important and highly non-trivial point to check is that we are able to reproduce our previous results obtained using the dedicated mode. This is indeed possible and in Fig. 1 we show the jet veto cross section, at full colour, for the process $q\bar{q} \rightarrow q\bar{q}$ in the case of back-to-back jets produced at $\pi/6$ to the collision axis in the zero momentum frame and with the veto region defined by the central region from $\pi/4 < \theta < 3\pi/4$. The colours used to represent each multiplicity will remain the same for the rest of this paper. We use the same notation as in the partner paper to label the colour-flow density matrix elements of

the hard scatter process, which we dress with soft gluon evolution. Specifically, $|01\rangle$ is the colour flow corresponding to s -channel singlet exchange and it is also the leading colour flow corresponding to t -channel gluon exchange, whereas $|10\rangle$ is the flow corresponding to t -channel singlet exchange and it is also the leading flow corresponding to s -channel gluon exchange.

For the $|10\rangle\langle 10|$ and $|10\rangle\langle 01|$ colour flow contributions to the hard scattering, we observe perfect agreement between the two modes (the solid and dash-dotted black curves coincide). This is especially non-trivial as the multiplicities build the cross section differently: in dedicated mode all emissions are out of gap, while in event generator mode emissions can be in any region. The event generator data was evolved down to an infrared scale $\mu = 0.1$, and to contribute to the cross section at $\rho = 0.1$ all emissions must have been out of the gap. Therefore, for the lowest ρ bin, the event generator mode and dedicated mode are equivalent. The reason for the disagreement at large ρ in the $|01\rangle\langle 01|$ case is due to missing contributions from higher multiplicities since we did not include ≥ 7 gluon emissions and this colour flow radiates more into the gap region. To avoid the need to consider more than 6 emissions, in what follows we always take $r = 0.3$, i.e. we always veto hard radiation emitted in the veto region. Note that there is no impediment to reducing μ and exploring lower values of ρ but we choose not to do so because $\rho > 0.1$ is sufficient to see clearly the impact of subleading colour.

3 Final state jets

In this section our focus is a $q\bar{q}q\bar{q}$ final state, as might occur in $ZZ \rightarrow$ jets. We fixed the kinematics in an asymmetric fashion and Fig. 2 shows the differential distribution of the highest energy soft gluon emitted into the veto region in events with exactly three emissions, i.e. the $n = 3$ contribution to Eq. (2.2). The veto region is defined as the region outside of the four cones, each with opening angle $\arccos(0.95)$, centred around the hard partons. We did not generate any more statistics for this process than the other processes we consider in this paper, so these plots are indicative that we are able to analyse full colour, soft radiation fully differentially without much trouble. The locations of the four hard partons are marked on the plot. The vertical pink line on the right corresponds to a quark emitted at $\theta = 0$, the green crosses are a quark emitted at $\theta = 11\pi/12$ and $\phi = 0$, the light blue cross is an anti-quark at $\theta = 2\pi/3$ and $\phi = \pi/12$ and the red cross is an anti-quark at $\theta = 3\pi/4$ and $\phi = \pi/4$. The colour-flow configurations are such that $|01\rangle$ corresponds to the pink (quark) and light blue (anti-quark) particles being colour connected (and also the green and red particles) whereas the $|10\rangle$ flow corresponds to the pink and red being connected (and the blue and green). The black regions surrounding the hard partons are the jet regions (over which we are fully inclusive), i.e. the regions complementary to the veto region. A noticeable feature is the strong radiation around $\cos\theta \sim 0.4$ between pink quark and light blue anti-quark in the $|01\rangle\langle 01|$ plot, which is much weaker for the $|10\rangle\langle 10|$ contribution. In the latter, the pink quark is colour connected to the red anti-quark, which shifts the radiation higher in ϕ . The radiation of the $|10\rangle\langle 01|$ interference contribution is an entirely subleading colour effect, because the interference density matrix cannot emit

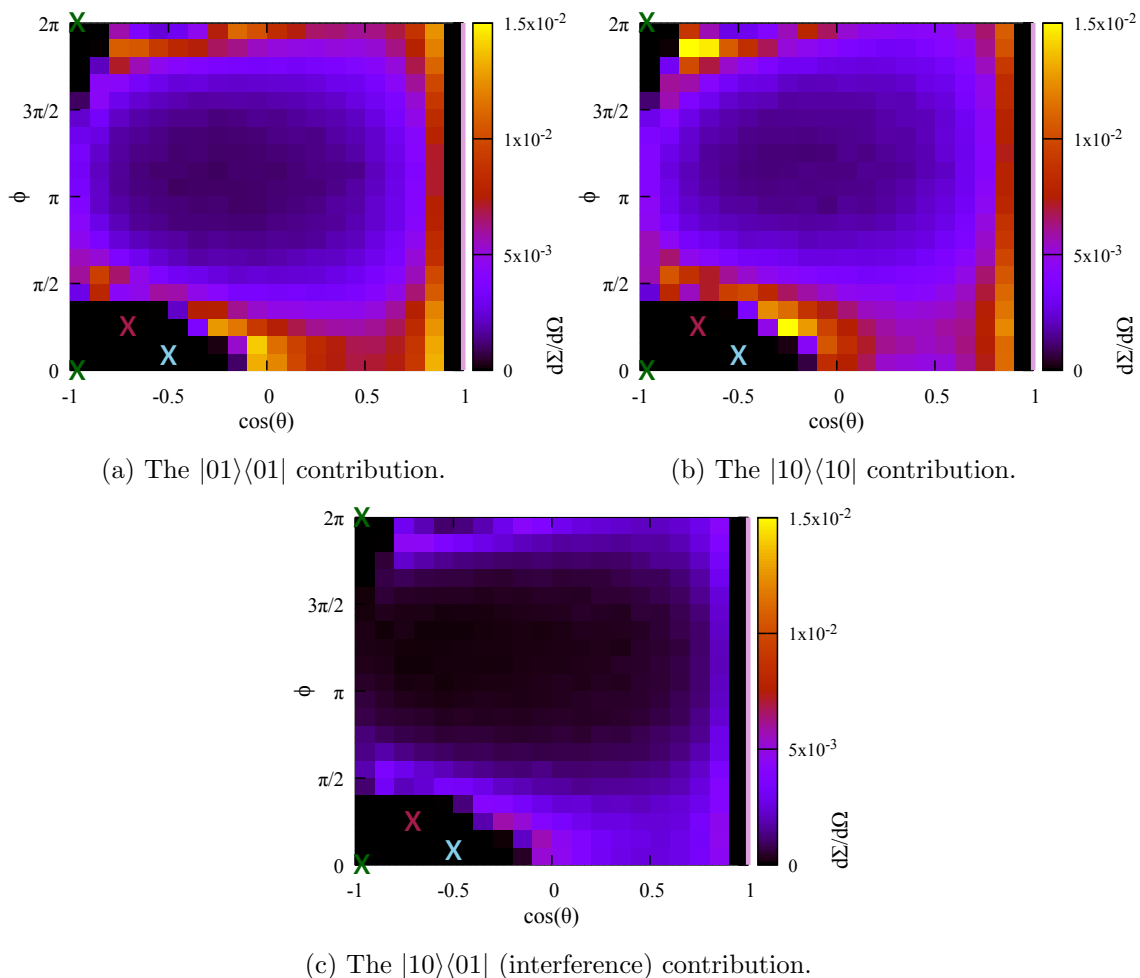


Figure 2: The full colour, three-gluon-emission differential cross section contribution to $d\Sigma/d\Omega$ for the $ZZ \rightarrow q\bar{q}q\bar{q}$ process. The locations of the hard jets are marked: the four crosses and the pink line. The black regions around the primary partons indicate the jet regions.

at leading colour. This quantity is of particular interest, since electroweak diboson final states at LEP2 have been considered as key tools to investigate colour reconnection models [7, 8], and the W mass extraction at future lepton colliders will rely on how well colour reconnection effects between the hadronic W systems are under control [9].

In Fig. 3 we show the cross section differential in the polar and azimuthal angles of the highest energy soft gluon emitted into the veto region, i.e. Eq. (2.3) and Eq. (2.4). We find that there is good agreement between leading and full colour results for the $|01\rangle\langle 01|$ and $|10\rangle\langle 10|$ contributions. However, the interference distributions have significantly different radiation patterns compared to the colour-diagonal contributions. In particular, the $d\Sigma/d\phi$ interference contribution is much steeper in the region away from the hard jets.

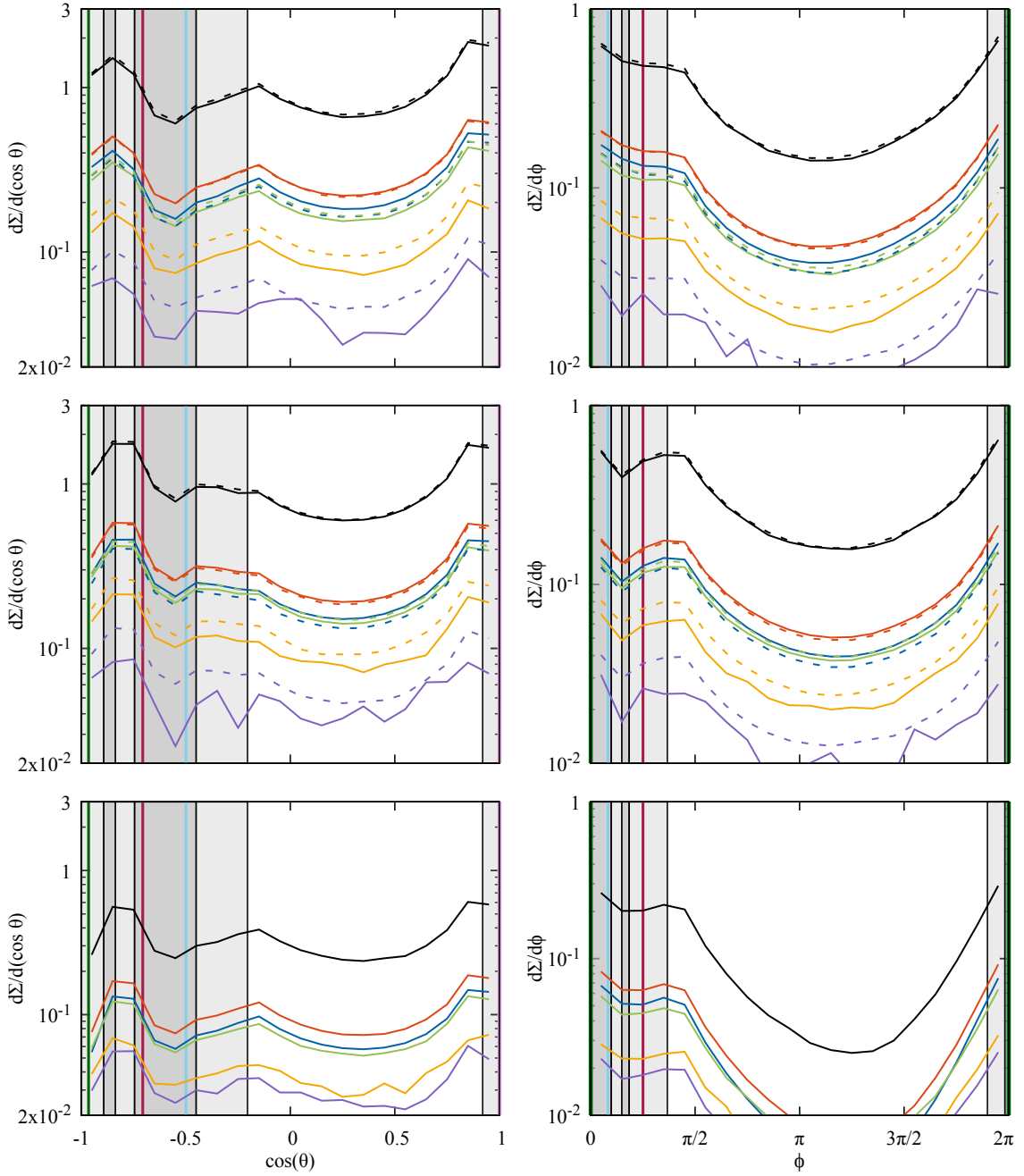


Figure 3: The differential cross sections for the different contributions to the $ZZ \rightarrow q\bar{q}q\bar{q}$ process, broken down by multiplicity. The top row is the $|01\rangle\langle 01|$ contribution, the middle row is the $|10\rangle\langle 10|$ contribution, and the bottom row is the $|10\rangle\langle 01|$ (interference) contribution. The solid curves are the full colour evolution, and the dashed curves are the leading colour evolution. For the interference case there is no leading colour contribution because there are no dipoles to emit from. The locations of the hard jets are marked with vertical lines matching the colours used in Fig. 2. The shaded vertical bars indicate the width of the cones around each hard parton. Darker shades indicate an overlap of multiple cones.

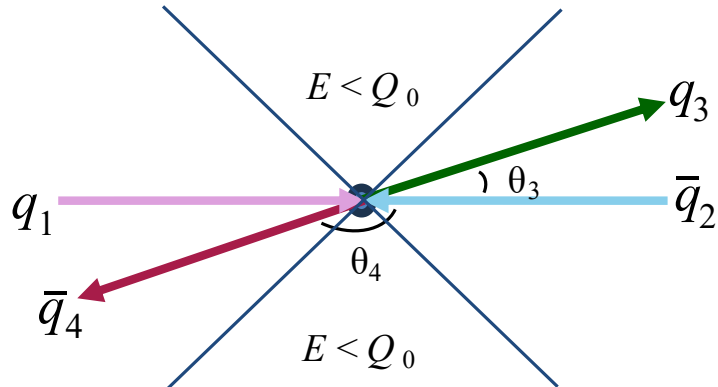


Figure 4: The kinematic configuration of the four hard partons in $q_1 \bar{q}_2 \rightarrow q_3 \bar{q}_4$. The angles of the different configurations considered are given in Table 1, and the veto region definitions for each configuration are given in the text. The colours of the four legs (pink q_1 , light blue \bar{q}_2 , dark green q_3 , red \bar{q}_4) are used in the figures to indicate the location of the hard partons. The colour state $|01\rangle$ corresponds to pink-light blue colour connected, and dark green-red connected. The colour state $|10\rangle$ corresponds to pink-dark green connected, and light blue-red connected.

	back-to-back		boosted		recoiling	
	θ	ϕ	θ	ϕ	θ	ϕ
q_1	0	0	0	0	0	0
\bar{q}_2	π	0	π	0	π	0
q_3	$\pi/6$	0	0.037	0	$\pi/6$	0
\bar{q}_4	$5\pi/6$	π	2.873	π	$\pi/3$	$19\pi/12$

Table 1: The directions of the quarks and anti-quarks for each of the kinematic configurations considered.

4 Hadronic jets

In this section our focus is the hard scattering $q\bar{q} \rightarrow q\bar{q}$, such as might occur in the collision of two hadrons. We consider three different kinematic configurations, as specified in Table 1. The back-to-back configuration corresponds to parton scattering in the zero momentum frame to produce jets in the forward and backward directions. In this case, the veto region is the central region satisfying $-0.8 < \cos\theta < 0.8$. The boosted configuration corresponds to a more extreme low-angle scattering with a boost along the collision axis. In this case, the veto region is the central region satisfying $-0.9 < \cos\theta < 0.9$. The recoiling configuration corresponds to the case where the outgoing partons are not back-to-back in azimuth, such as would occur if the jets are recoiling against a colourless particle (e.g.

as in the case of weak vector boson fusion at the LHC). In this case, the veto region is defined to be the region outside of jets defined by cones centred on the final state quark and anti-quark, each with opening angle $\arccos(0.95)$.

In what follows, we will show results arising from the $|01\rangle\langle 01|$ and $|10\rangle\langle 10|$ hard process density matrices, and also the combinations corresponding to t -channel and s -channel gluon exchange. The $|01\rangle\langle 01|$ colour configuration corresponds to the incoming particles being colour connected and the outgoing particles being colour connected. The $|10\rangle\langle 10|$ configuration corresponds to the incoming quark connected to the outgoing quark and equivalently for the antiquarks.

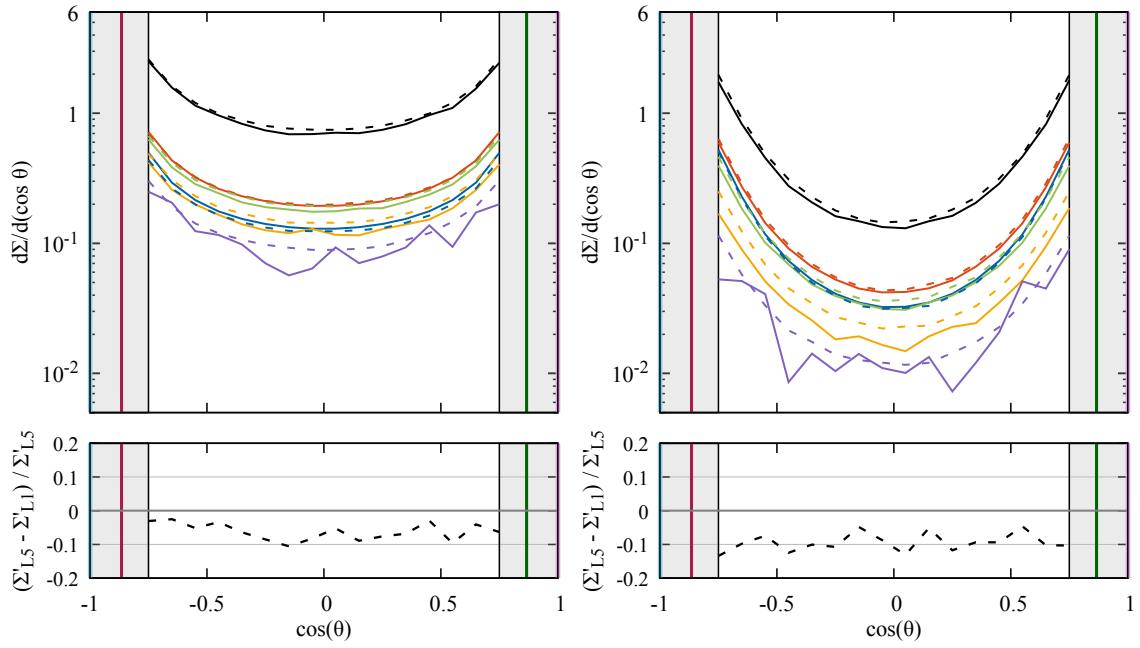
For each contribution we show the result of full colour evolution compared to the result of strictly leading colour evolution. For the s - and t - channel gluon exchange contributions, we initiate the leading colour evolution using the leading-colour part of the hard-scatter matrix. This is what we referred to as the L1, LCH approximation in the partner paper and we have chosen it here since that is generally the best performing approximation to the full colour result for the gaps-between-jets observable: specifically, we found that L1, LCH showed very good agreement with the full colour result for t -channel gluon exchange in every $2 \rightarrow 2$ scattering process we considered (as first observed in [10, 11]). By analysing the soft radiation differentially, we aim to stress-test the success of this remarkable approximation.

4.1 Back-to-back jets

The $d\Sigma/d(\cos\theta)$ distributions are shown in Fig. 5. As expected, we see the radiation grows as it gets closer to the hard jets (their location is indicated with vertical lines matching the colours in Fig. 4). The $|01\rangle\langle 01|$ distribution is less steep than $|10\rangle\langle 10|$, which follows from the colour flows: in the former configuration, the colour-connected pairs are back-to-back, which causes them to emit in all directions, including the veto region. In contrast, $|10\rangle\langle 10|$ has the connected pairs at angles of $\pi/6$, which leads to most of the radiation being emitted out of the veto region, and results in a much steeper radiation pattern.

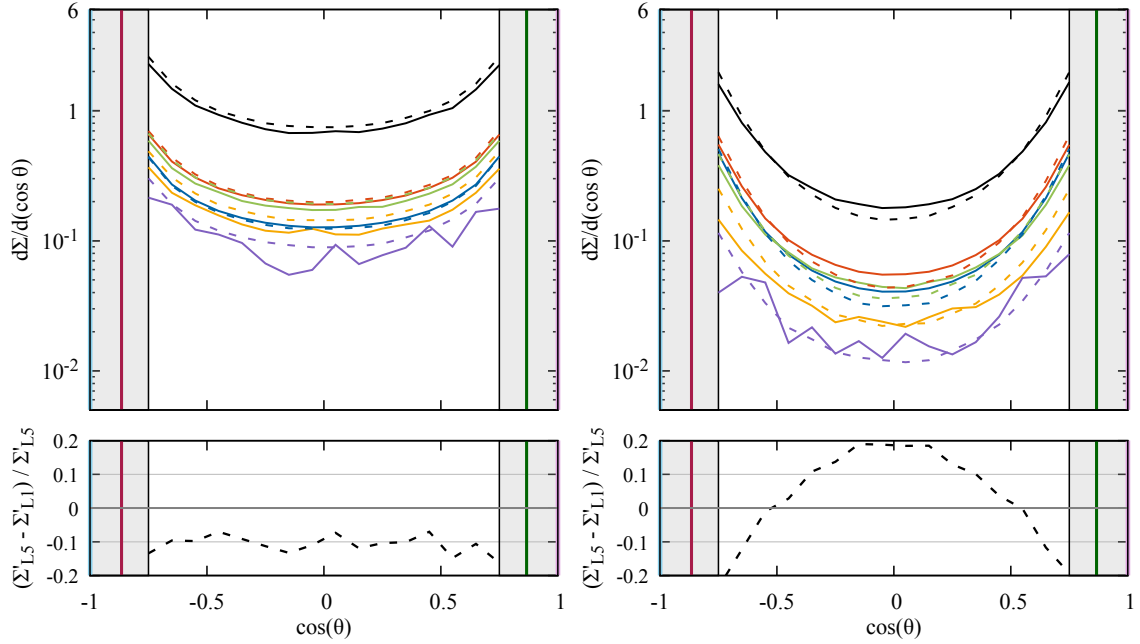
Since the strictly leading colour and full colour results have different normalisations, we should focus on the shape of the residuals. We see that the residual for the $|10\rangle\langle 10|$ contribution is approximately flat. In contrast, the residual for the $|01\rangle\langle 01|$ shows a 5-10% effect between the edges and centre of the veto region, although we have some fluctuations. It is perhaps easier to see this effect by looking at the 1, 2 or 3 emission curves (blue, orange, light green respectively). The effect is caused by virtual gluon exchange causing swaps to the $|10\rangle\langle 10|$ configuration, which radiates more outside of the veto region, therefore enhancing the differential cross section near the edges of the veto region relative to the centre. That said, we have a clearer example in the next section.

The t -channel gluon exchange contribution has a flat residual, showing that those subleading-colour effects in the $|01\rangle\langle 01|$ evolution cancel, but only after also including the interference contribution, shown in Fig. 6, and the subleading $|10\rangle\langle 10|$ contribution. This is despite the fact that the interference evolution vanishes at leading colour. Moreover, the radiation pattern from the interference contribution has a very different shape (steeper) compared to those of the $|01\rangle\langle 01|$ and $|10\rangle\langle 10|$ contributions.



(a) The $|01\rangle\langle 01|$ contribution.

(b) The $|10\rangle\langle 10|$ contribution.



(c) The t -channel gluon exchange contribution. (d) The s -channel gluon exchange contribution.

Figure 5: The differential cross section $d\Sigma/d(\cos\theta)$ of the different contributions to the $q\bar{q} \rightarrow q\bar{q}$ process, in the back-to-back configuration, and broken down by multiplicity. The solid curves are obtained using full colour evolution, and the dashed curves use strictly leading colour evolution. For the leading colour curves, we start the evolution using the leading-colour approximation to the hard-scatter density matrix. The locations of the hard jets are marked with vertical lines matching the colours used in Fig. 4. The shaded vertical bars indicate the jet regions.

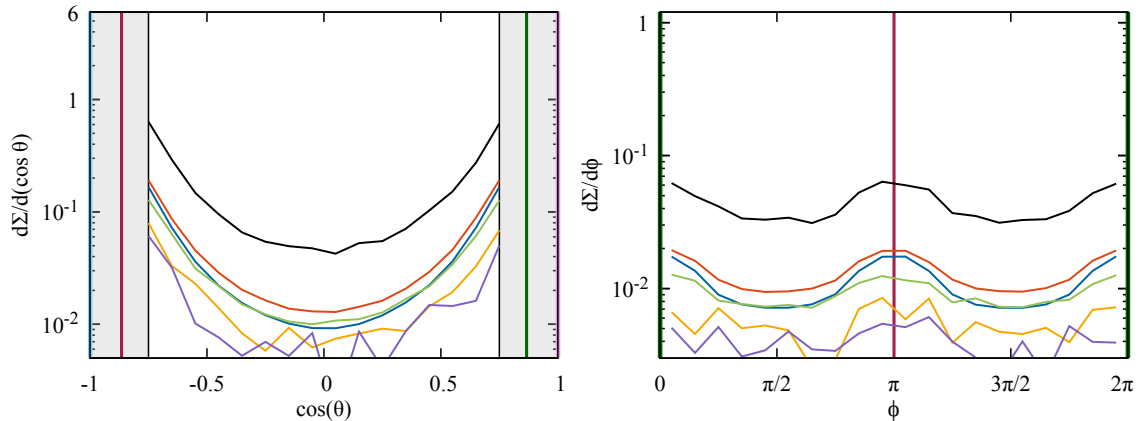


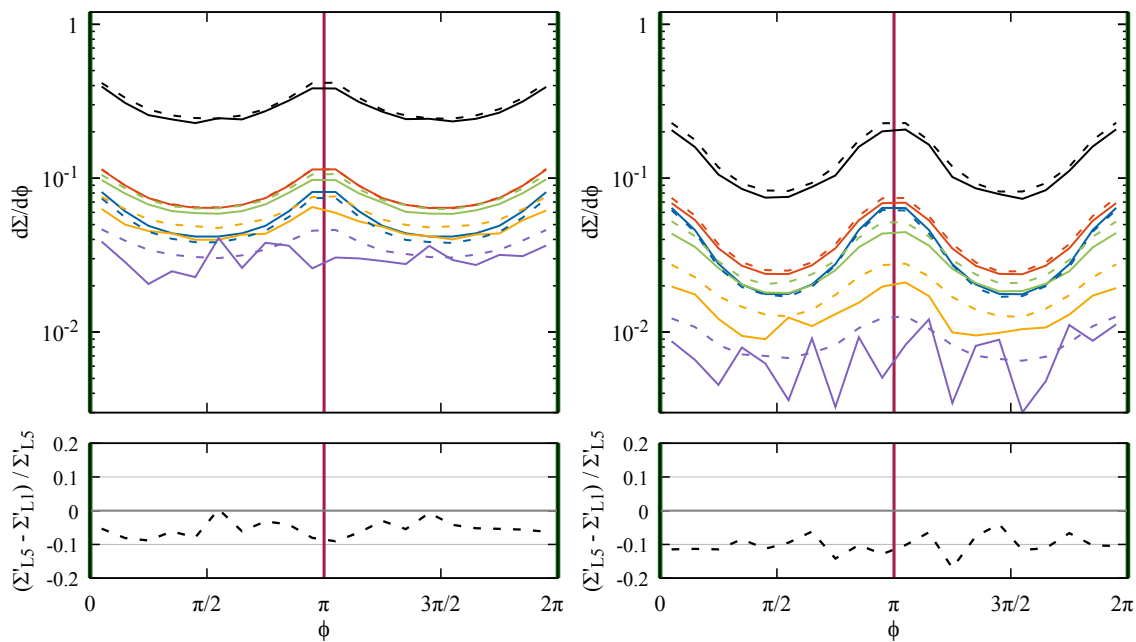
Figure 6: The differential cross sections arising from the $|10\rangle\langle 01|$ (interference) contribution to the $q\bar{q} \rightarrow q\bar{q}$ process, in the back-to-back configuration, and broken down by multiplicity. The solid curves are obtained using full colour evolution. There is no leading colour contribution since there are no dipoles to emit from. The locations of the hard jets are marked with vertical lines matching the colours used in Fig. 4. The shaded vertical bars indicate the jet regions.

The s -channel contribution shows the largest discrepancy between the full colour and leading colour results. The inclusion of the subleading $|01\rangle\langle 01|$ and $|10\rangle\langle 01|$ interference contributions flattens the full colour radiation pattern, causing an overall 40% effect between the edges and the middle of the veto region.

We show the $d\Sigma/d\phi$ distributions in Fig. 7. The positions in ϕ of the two outgoing particles are shown with vertical lines on the plot. Again, we see that the $|01\rangle\langle 01|$ contribution radiates more evenly in ϕ than the $|10\rangle\langle 10|$ contribution, which prioritises radiation along the directions of the two colour-connected pairs. The $|10\rangle\langle 10|$ residual is approximately flat, while the $|01\rangle\langle 01|$ residual shows $\sim 5\%$ effects between the edges and centre of the veto region. The t -channel residual is approximately flat, although with fluctuations, while the s -channel residual shows $\sim 10\%$ effects.

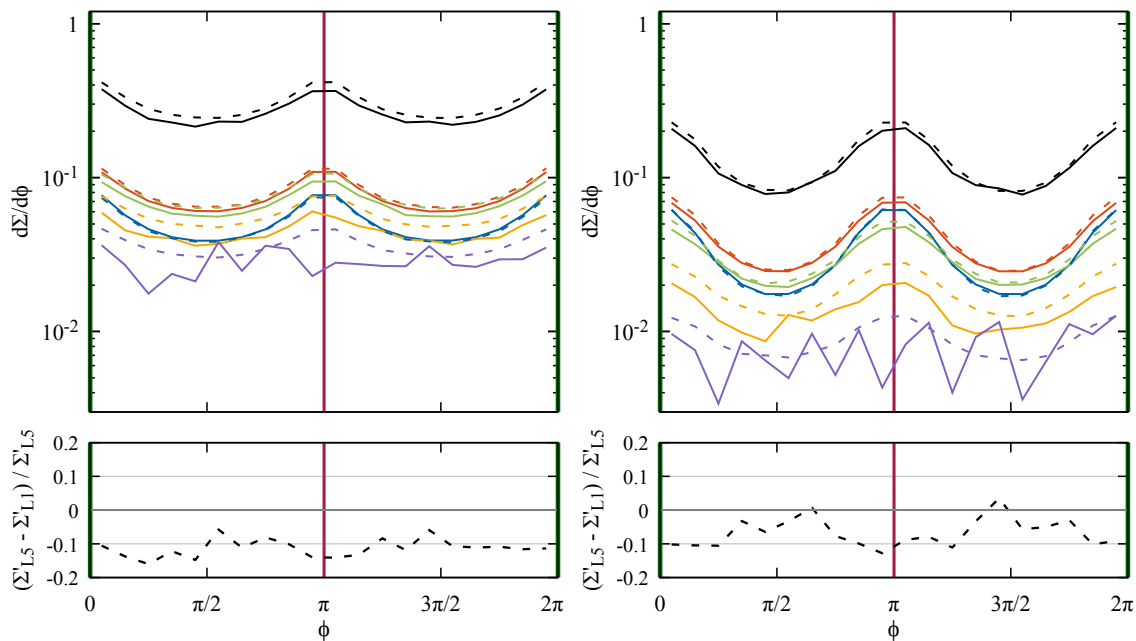
4.2 Jets with a boost

We next consider the boosted jets kinematic configuration. The $d\Sigma/d(\cos\theta)$ distribution in Fig. 8 clearly shows the effect of the small, and asymmetric, scattering angles: the $|10\rangle\langle 10|$ contribution is now highly asymmetric in θ . The q_1 - q_3 opening angle is much smaller than the \bar{q}_2 - \bar{q}_4 opening angle, suppressing radiation from the former dipole and enhancing it from the latter. On the other hand, the $|01\rangle\langle 01|$ contribution, where the colour-connected pairs are almost back-to-back, remains more symmetric, but not completely: full colour evolution can lead to virtual gluon exchanges that swap from this colour configuration to the other, which visibly enhances the full colour curves towards $\cos\theta = -1$. This is most visible for the one-emission curve (solid blue), but is present for all multiplicities. The $|10\rangle\langle 10|$ evolution emits mostly outside the veto region, and therefore disfavours swapping to a different colour configuration.



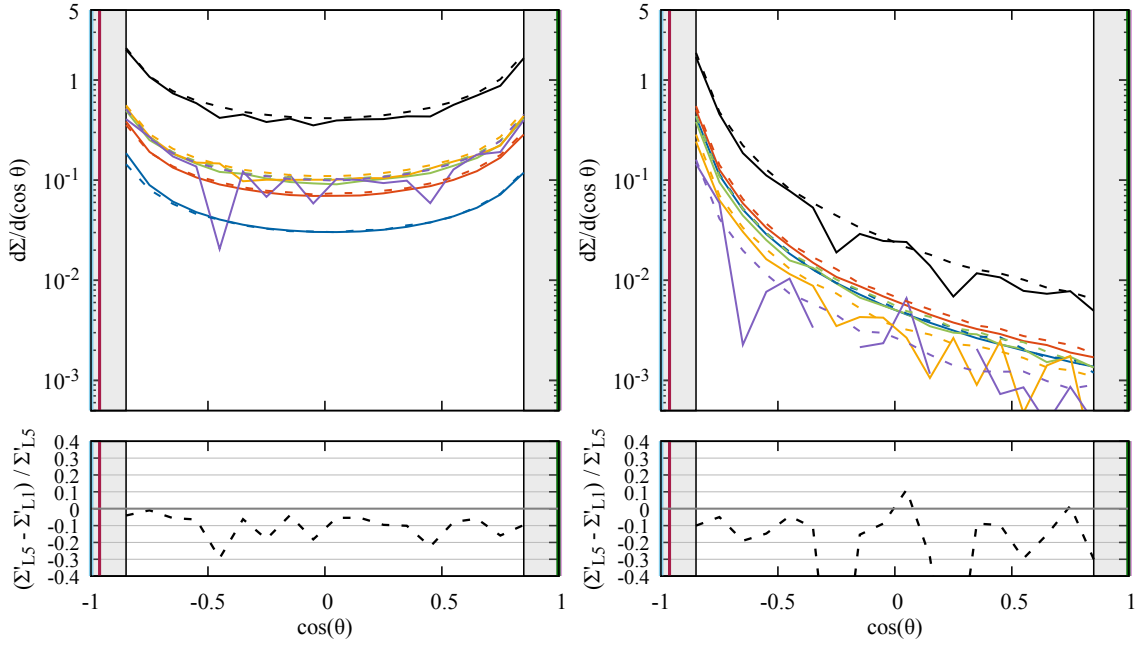
(a) The $|01\rangle\langle 01|$ contribution.

(b) The $|10\rangle\langle 10|$ contribution.



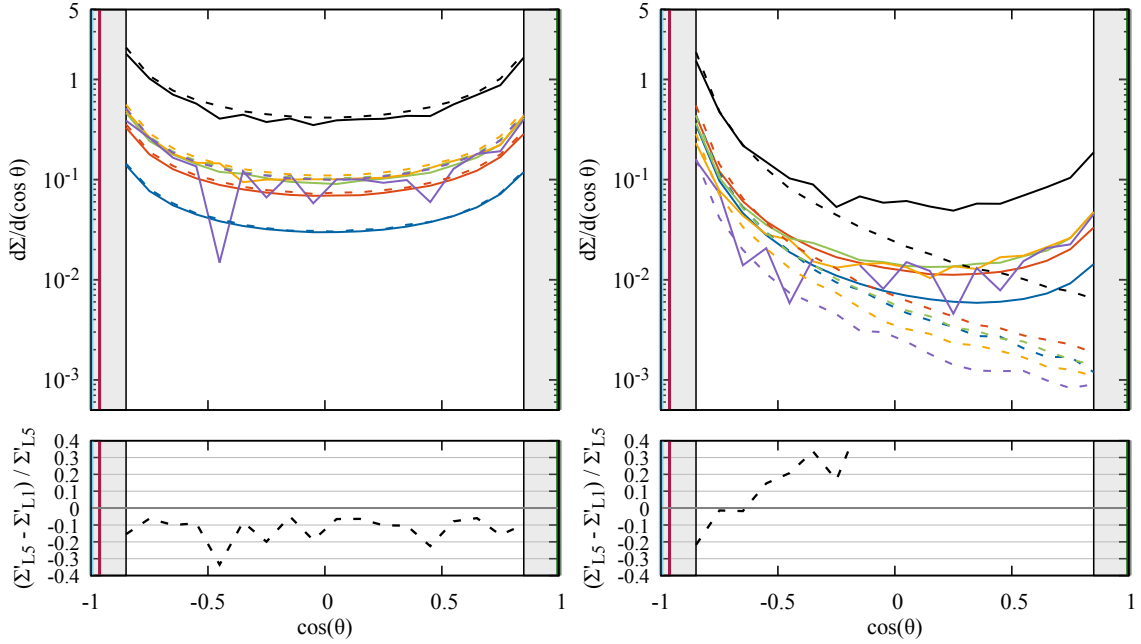
(c) The t -channel gluon exchange contribution. (d) The s -channel gluon exchange contribution.

Figure 7: The differential cross section $d\Sigma/d\phi$ of the different contributions to the $q\bar{q} \rightarrow q\bar{q}$ process, in the back-to-back configuration, and broken down by multiplicity. The solid curves are obtained using full colour evolution, and the dashed curves use strictly leading colour evolution. For the leading colour curves, we start the evolution using the leading-colour approximation to the hard-scatter density matrix. The locations of the hard jets are marked with vertical lines matching the colours used in Fig. 4.



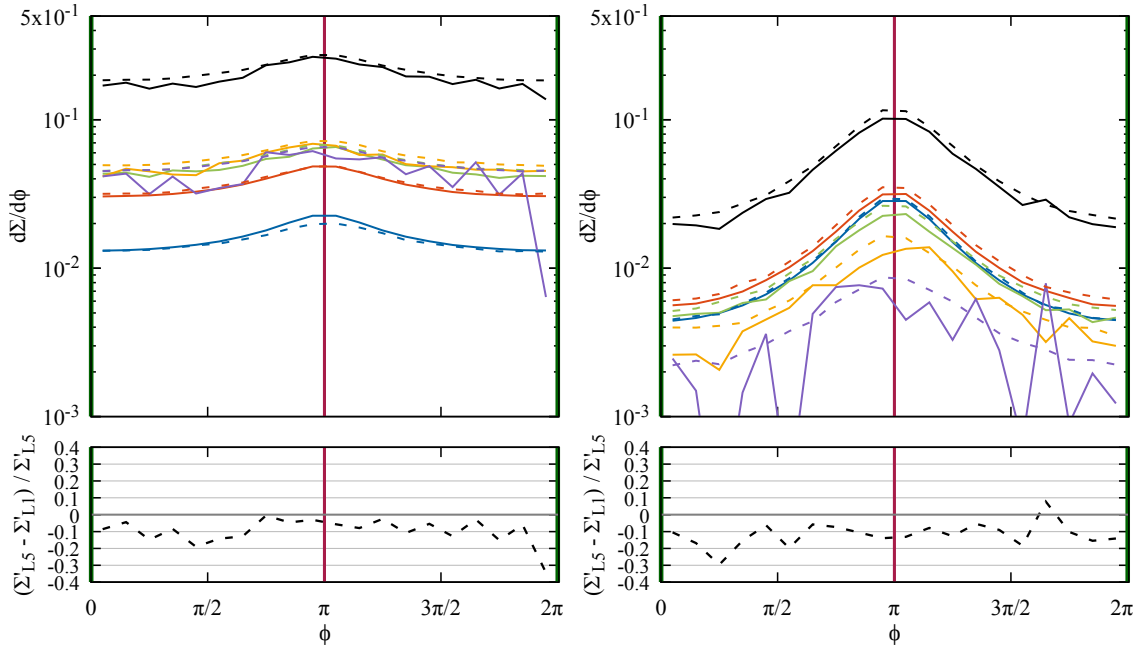
(a) The $|01\rangle\langle 01|$ contribution.

(b) The $|10\rangle\langle 10|$ contribution.



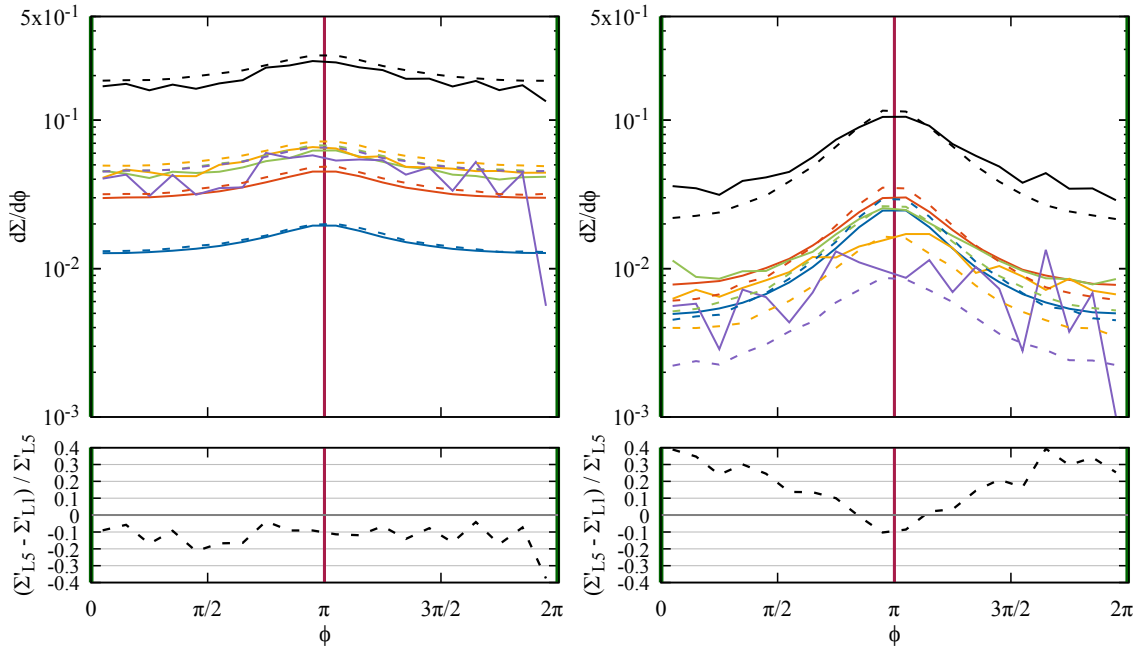
(c) The t -channel gluon exchange contribution. (d) The s -channel gluon exchange contribution.

Figure 8: The differential cross section $d\Sigma/d(\cos\theta)$ of the different contributions to the $q\bar{q} \rightarrow q\bar{q}$ process, in the boosted jets configuration, and broken down by multiplicity. The solid curves are obtained using full colour evolution, and the dashed curves use strictly leading colour evolution. For the leading colour curves, we start the evolution using the leading-colour approximation to the hard-scatter density matrix. The locations of the hard jets are marked with vertical lines matching the colours used in Fig. 4. The shaded vertical bars indicate the jet regions.



(a) The $|01\rangle\langle 01|$ contribution.

(b) The $|10\rangle\langle 10|$ contribution.



(c) The t -channel gluon exchange contribution. (d) The s -channel gluon exchange contribution.

Figure 9: The differential cross section $d\Sigma/d\phi$ of the different contributions to the $q\bar{q} \rightarrow q\bar{q}$ process, in the boosted jets configuration, and broken down by multiplicity. The solid curves are obtained using full colour evolution, and the dashed curves use strictly leading colour evolution. For the leading colour curves, we start the evolution using the leading-colour approximation to the hard-scatter density matrix. The locations of the hard jets are marked with vertical lines matching the colours used in Fig. 4.

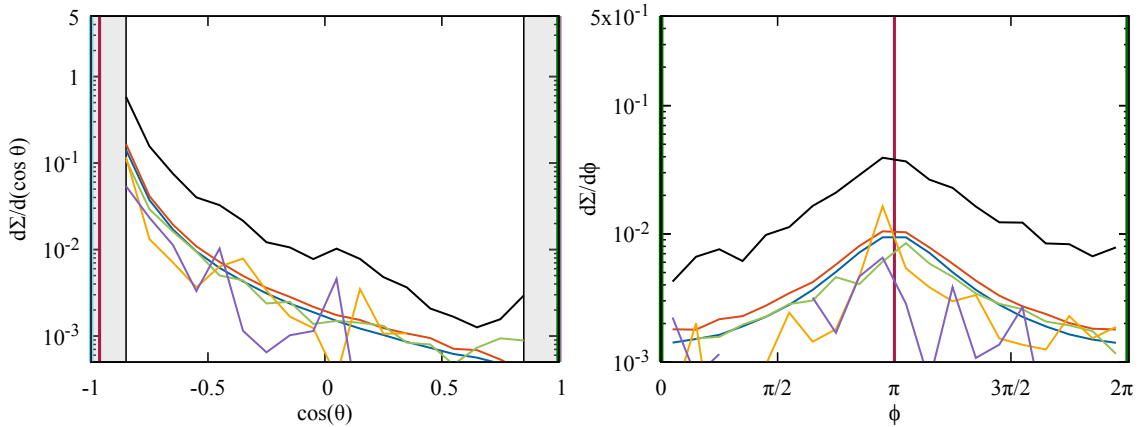


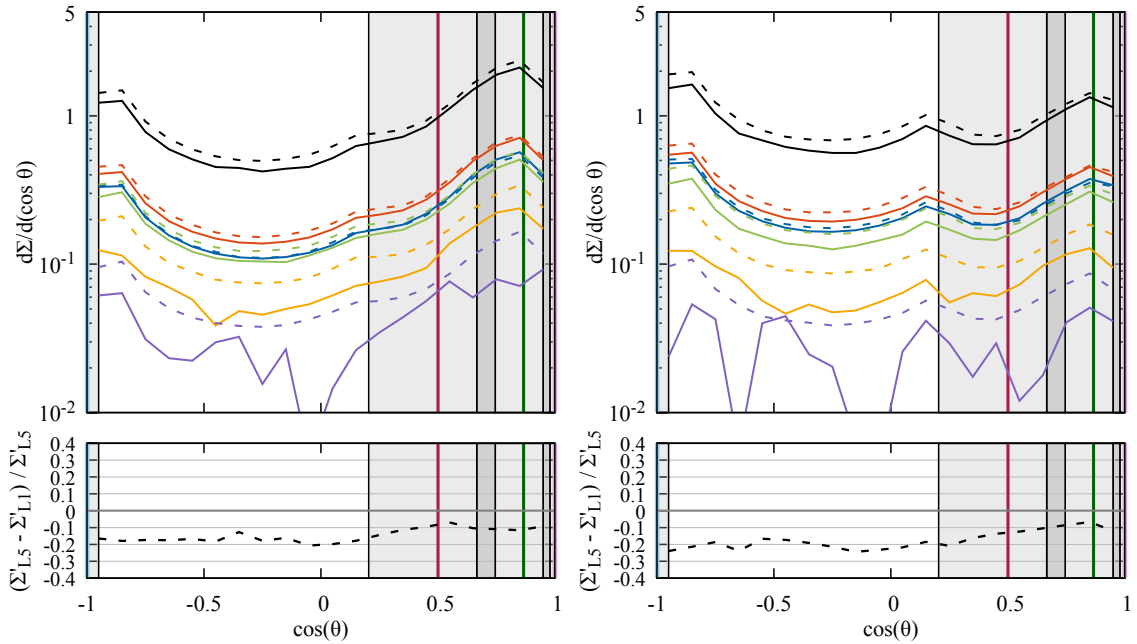
Figure 10: The differential cross sections arising from the $|10\rangle\langle 01|$ (interference) contribution to the $q\bar{q} \rightarrow q\bar{q}$ process, in the boosted jets configuration, and broken down by multiplicity. The solid curves are obtained using full colour evolution. There is no leading colour contribution since there are no dipoles to emit from. The locations of the hard jets are marked with vertical lines matching the colours used in Fig. 4. The shaded vertical bars indicate the jet regions.

The s -channel gluon exchange contribution is very different between full and leading colour, as the latter is unable to swap into the $|01\rangle\langle 01|$ configuration. Interestingly, the t -channel, full colour result once again exhibits the cancellation of the small enhancement near $\cos\theta = -1$ from the $|10\rangle\langle 10|$ evolution with the interference (Fig. 10) and the sub-leading $|10\rangle\langle 10|$ contributions.

The azimuthal distributions are shown in Figs. 9 and the interference distributions are shown in Fig. 10. We note that all show the same characteristics: the $|10\rangle\langle 10|$ contribution shows very good agreement between full and leading colour; the $|01\rangle\langle 01|$ contribution shows full colour enhances the radiation in the region near the hard jets; s -channel gluon exchange completely fails to be described by leading colour evolution; t -channel gluon exchange demonstrates that the enhancement in $|01\rangle\langle 01|$ cancels with the $|10\rangle\langle 10|$ and interference contributions, resulting in the surprisingly good agreement between full colour and leading colour.

4.3 Jets with a recoil

We conclude by considering the case where the jets are produced with a recoil, such as may occur in vector boson fusion to produce a Higgs or a pair of weak bosons at the LHC. In this configuration both final state jets point in the general direction of the incoming q_1 , thus not favouring any particular colour configuration. The goal is to test whether this will spoil the agreement between full colour and leading colour for the radiation patterns of the t -channel gluon exchange. We find the evolution of the individual $|01\rangle\langle 01|$ and $|10\rangle\langle 10|$ contributions do not show any remarkable features, likely due to the angles of the connected pairs being of similar sizes, so we omit them for brevity. Instead, we focus on the s - and t -channel gluon exchange contributions, in Figs. 11 and 12.



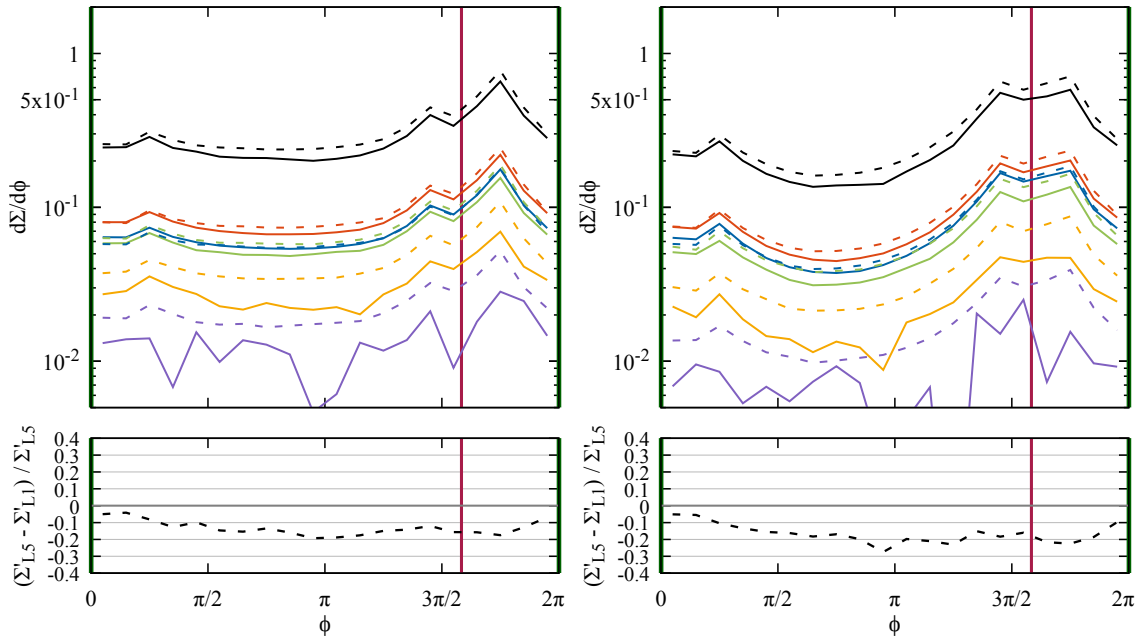
(a) The t -channel gluon exchange contribution. (b) The s -channel gluon exchange contribution.

Figure 11: The differential cross section $d\Sigma/d(\cos\theta)$ of the different contributions to the $q\bar{q} \rightarrow q\bar{q}$ process, in the jets with a recoil configuration, and broken down by multiplicity. The solid curves are obtained using full colour evolution, and the dashed curves use strictly leading colour evolution. For the leading colour curves, we start the evolution using the leading-colour approximation to the hard-scatter density matrix. The locations of the hard jets are marked with vertical lines matching the colours used in Fig. 4. The shaded vertical bars indicate the jet regions. Darker shades indicate an overlap of multiple jet-cones.

In general, we find that the full colour cross section is enhanced by $\sim 10\%$ relative to the leading colour one in the region near the three closer jets q_1 , q_3 , and \bar{q}_4 for both gluon exchange channels. This is clearly visible in Fig. 11. We also observe significantly different radiation distributions between full and leading colour, which are most clearly visible by looking at individual multiplicities. For example, in Fig. 12, t -channel gluon exchange, the two-emission orange curves have different shapes. There are multiple competing colour configurations that radiate in this region, which might explain why full colour evolution, which can access all configurations, may enhance radiation. This kinematic configuration provides us with a case where the strictly leading colour approximation for hard processes involving t -channel gluon exchange fails.

5 Conclusions and outlook

We have investigated the full colour evolution of jet processes differentially in the inter-jet radiation. This study provides crucial insight into how subleading colour effects affect



(a) The t -channel gluon exchange contribution. (b) The s -channel gluon exchange contribution.

Figure 12: The differential cross section $d\Sigma/d\phi$ of the different contributions to the $q\bar{q} \rightarrow q\bar{q}$ process, in the jets with a recoil configuration, and broken down by multiplicity. The solid curves are obtained using full colour evolution, and the dashed curves use strictly leading colour evolution. For the leading colour curves, we start the evolution using the leading-colour approximation to the hard-scatter density matrix. The locations of the hard jets are marked with vertical lines matching the colours used in Fig. 4.

collider observables beyond the rather inclusive gaps-between-jets measurements, which sometimes turn out to be sensitive to subleading colour only via an overall normalization. In fact, we generally find that there are intricate radiation patterns between jets, and some of the full colour effects cancel in observables only upon integrating over large enough patches of solid angle. Our intention is to follow up this study by looking at more differential observables, including full collider cross sections involving the entire hard-scatter matrix elements, and to also assess the impact of Coulomb exchanges, which we are able to compute using `CVolver`, as demonstrated in the appendix. At future lepton colliders multi-jet final states, such as those originating from hadronic decays of electroweak final states, will be affected by sub-leading colour, and we have calculated the $1/N_c^2$ suppressed interference contribution. It will be interesting to confront this with existing colour reconnection models, in particular those motivated by soft gluon evolution [12, 13]. Ultimately, it is desirable that colour reconnection and hadronization models be studied in the context of full colour evolution [5]. For the future, it remains for us to include hard-collinear physics in `CVolver`, which will allow us to describe collinear sensitive observables as detailed in [5, 6].

A Coulomb gluon exchange

There is very considerable interest in exploring the role played by Coulomb (Glauber) gluons in QCD scattering processes. The discovery of super-leading logarithms [14, 15] and the related breakdown of soft-collinear factorization [16–18] has led to progress in computing and resumming super-leading logarithms [19–22] including a first demonstration of their numerical importance in hadron-hadron collisions [23]. At present, `CVolver` is able to include Coulomb exchanges in the soft anomalous dimension, however due to the fact that we do not include hard-collinear physics the super-leading logarithms will formally diverge (in fact they grow logarithmically with the collinear cutoff). In Fig. 13 we show the effect of turning Coulomb exchanges on, first in $Z \rightarrow q\bar{q}$, which has a colourless initial state, and also in $q\bar{q} \rightarrow q\bar{q}$. In both cases we consider the back-to-back kinematic configuration considered in the main text and we show results for different values of the collinear cutoff. We see clearly the non-trivial cancellation of Coulomb exchanges in the former and their non-cancellation in the latter. Fig. 14 is the residual plot $q\bar{q} \rightarrow q\bar{q}$ and we can see that the result is collinear cutoff independent at these relatively high values of ρ . We do not expect this to persist to low values of ρ .

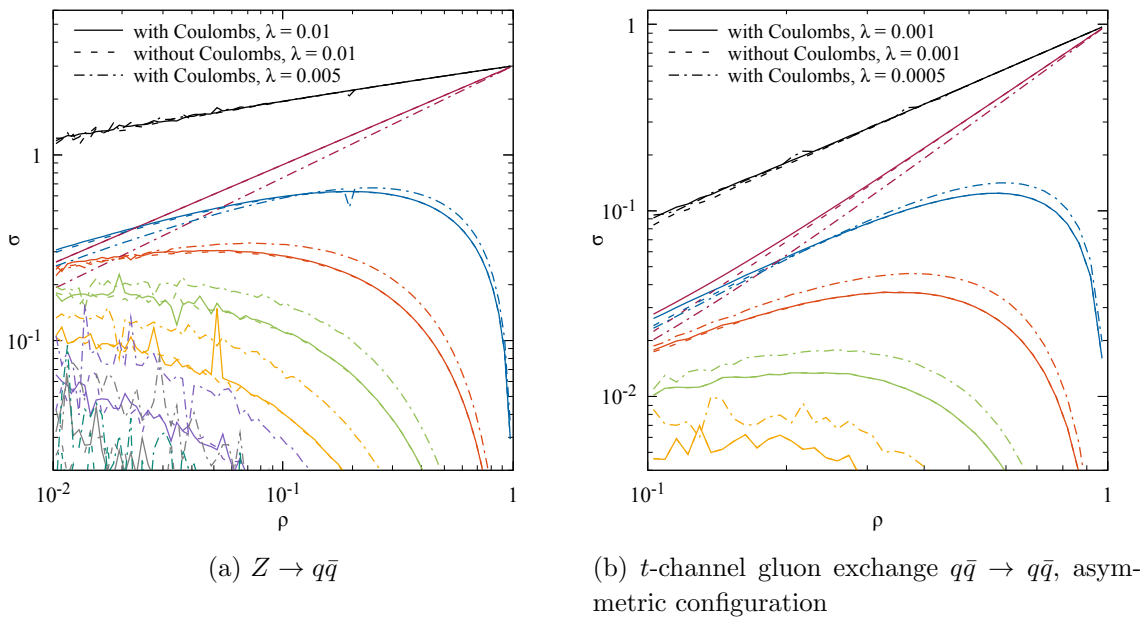


Figure 13: Testing the impact of including Coulomb gluons.

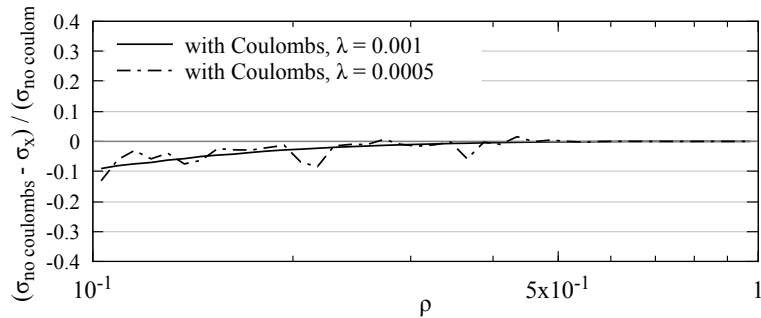


Figure 14: Including Coulombs in $q\bar{q} \rightarrow q\bar{q}$ induces a 10% effect at $\rho = 0.1$

Acknowledgments

This work has received funding from the U.K. Science and Technology Facilities Council grant no. ST/X00077X/1. FTG is supported by the Royal Society through Grant URF/R1/201500. We thank Jack Holguin for fruitful discussions, and Matthew De Angelis for earlier contributions to the program. The numerical results presented in this paper have been obtained on the computing clusters of the Particle Physics Groups of Universität Wien and The University of Manchester. We are grateful for having been able to use these facilities. FTG acknowledges the kind hospitality of the Theoretical Physics Group of the Institute of Physics of the Universität Graz.

References

- [1] J.R. Forshaw, S. Plätzer and F. Torre González, *Exact colour evolution for jet observables*, [2502.12133](#).
- [2] S. Plätzer, *Summing Large- N Towers in Colour Flow Evolution*, *Eur. Phys. J. C* **74** (2014) 2907 [[1312.2448](#)].
- [3] M. De Angelis, J.R. Forshaw and S. Plätzer, *Resummation and Simulation of Soft Gluon Effects beyond Leading Color*, *Phys. Rev. Lett.* **126** (2021) 112001 [[2007.09648](#)].
- [4] R. Ángeles Martínez, M. De Angelis, J.R. Forshaw, S. Plätzer and M.H. Seymour, *Soft gluon evolution and non-global logarithms*, [1802.08531](#).
- [5] S. Plätzer, *Colour evolution and infrared physics*, *JHEP* **07** (2023) 126 [[2204.06956](#)].
- [6] J.R. Forshaw, J. Holguin and S. Plätzer, *Parton branching at amplitude level*, *JHEP* **08** (2019) 145 [[1905.08686](#)].
- [7] L3 collaboration, *Search for color reconnection effects in $e^+e^- \rightarrow W^+W^- \rightarrow$ hadrons through particle flow studies at LEP*, *Phys. Lett. B* **561** (2003) 202 [[hep-ex/0303042](#)].
- [8] DELPHI collaboration, *Investigation of colour reconnection in WW events with the DELPHI detector at LEP-2*, *Eur. Phys. J. C* **51** (2007) 249 [[0704.0597](#)].
- [9] J. de Blas et al., *Focus topics for the ECFA study on Higgs / Top / EW factories*, [2401.07564](#).
- [10] Y. Hatta and T. Ueda, *Resummation of non-global logarithms at finite N_c* , *Nucl. Phys.* **B874** (2013) 808 [[1304.6930](#)].

- [11] Y. Hatta and T. Ueda, *Non-global logarithms in hadron collisions at $N_c = 3$* , *Nucl. Phys. B* **962** (2021) 115273 [2011.04154].
- [12] S. Gieseke, P. Kirchga e er and S. Pl atzer, *Baryon production from cluster hadronisation*, *Eur. Phys. J. C* **78** (2018) 99 [1710.10906].
- [13] S. Gieseke, P. Kirchga e er, S. Pl atzer and A. Siodmok, *Colour Reconnection from Soft Gluon Evolution*, *JHEP* **11** (2018) 149 [1808.06770].
- [14] J.R. Forshaw, A. Kyrieleis and M.H. Seymour, *Super-leading logarithms in non-global observables in QCD*, *JHEP* **08** (2006) 059 [hep-ph/0604094].
- [15] J.R. Forshaw, A. Kyrieleis and M.H. Seymour, *Super-leading logarithms in non-global observables in QCD: Colour basis independent calculation*, *JHEP* **09** (2008) 128 [0808.1269].
- [16] S. Catani, D. de Florian and G. Rodrigo, *Space-like (versus time-like) collinear limits in QCD: Is factorization violated?*, *JHEP* **07** (2012) 026 [1112.4405].
- [17] J.R. Forshaw, M.H. Seymour and A. Si odmok, *On the Breaking of Collinear Factorization in QCD*, *JHEP* **11** (2012) 066 [1206.6363].
- [18] M.D. Schwartz, K. Yan and H.X. Zhu, *Collinear factorization violation and effective field theory*, *Phys. Rev.* **D96** (2017) 056005 [1703.08572].
- [19] J. Keates and M.H. Seymour, *Super-leading logarithms in non-global observables in QCD: Fixed order calculation*, *JHEP* **04** (2009) 040 [0902.0477].
- [20] T. Becher, M. Neubert and D.Y. Shao, *Resummation of Super-Leading Logarithms*, *Phys. Rev. Lett.* **127** (2021) 212002 [2107.01212].
- [21] T. Becher, M. Neubert, D.Y. Shao and M. Stillger, *Factorization of non-global LHC observables and resummation of super-leading logarithms*, *JHEP* **12** (2023) 116 [2307.06359].
- [22] P. B oer, P. Hager, M. Neubert, M. Stillger and X. Xu, *Renormalization-group improved resummation of super-leading logarithms*, *JHEP* **08** (2024) 035 [2405.05305].
- [23] T. Becher, P. Hager, G. Martinelli, M. Neubert, D. Schwienbacher and M. Stillger, *Super-leading logarithms in $pp \rightarrow 2$ jets*, *JHEP* **01** (2025) 171 [2411.12742].